Article

Not peer-reviewed version

Atomic Structure Calculations of Zr I-IV for Kilonova Modelling

Matteo Bezmalinovich *

Posted Date: 17 April 2026

doi: 10.20944/preprints202604.1298.v1

Keywords: kilonova; atomic data; opacity

 doi:10.20944/preprints202604.1298.v1

Article

Atomic Structure Calculations of Zr I-IV for Kilonova Modelling

Matteo Bezmalinovich [1,2]

[1] National Institute for Astrophysics – Astronomical Observatory of Abruzzo, Via Maggini snc, 64100, Teramo, Italy; matteo.bezmalinovich@inaf.it
[2] National Institute for Nuclear Physics – Section of Perugia, Via A. Pascoli, Perugia, Italy

Abstract

The optical counterpart of the gravitational wave event GW170817, known as kilonova, has provided strong evidence that binary neutron star mergers are favourable sites to host the r-process nucleosynthesis. Kilonova is a quasi-thermal electromagnetic emission powered by the radioactive decay of heavy neutron-rich nuclei produced by the r-process. Considering the variety of elements contributing to kilonova ejecta, essential information about its composition can be achieved through spectral characterisation, radiative transfer simulations, and opacities. The latter represents one of the most challenging aspects of the modelling, as it relies on accurate atomic structure calculations of energy levels and transitions. Since light r-process elements are major opacity contributors in early (< 2 days) scenario, this work focuses on atomic calculations for Zr I-IV. Energy levels and bound-bound transitions are determined using the `GRASP2018` code, assuming two different multi-reference sets for each ionisation stage: one including, and one excluding core-core and core-valence correlations. Results demonstrate that the inclusion of f shell and core correlations impacts on both energy levels and transitions. A systematic assessment of the accuracy is performed through detailed comparisons with the `NIST ASD`. Finally, these Zr data are integrated on the open access `MARTINI` platform.

Keywords: kilonova; atomic data; opacity

1. Introduction

The gravitational wave event GW170817 was a watershed moment for astronomy, marking the beginning of the era of multi-messenger astronomy [1,2]. Besides the confirmation of general relativity predictions, GW170817 also provided answers to the origins of heavy elements in the Universe. Since 1974 [3], binary neutron star (BNS) and black hole-neutron star mergers have long been hypothesised as possible candidates to host the heavy element nucleosynthesis through the rapid neutron capture process (r-process) [4]. With the coalescence of BNS observed in 2017, this hypothesis has now been confirmed.

GW170817 is considered a milestone for the community also because, for the first time, it was possible to observe gravitational waves together with electromagnetic (EM) counterparts. Specifically, GW170817 was accompanied by a short gamma-ray burst (GRB170817A) [5–7] and an EM transient: the kilonova (KN; AT2017gfo) [8–14]. Kilonova is a quasi-thermal transient powered by radioactive decay of heavy neutron rich isotopes synthesised through the r-process, shortly after mass ejection of compact mergers [15–17]. Here, neutron-rich material is ejected at fractions of the speed of light and undergoes r-process nucleosynthesis. The produced heavy elements rapidly decay for instability, powering the surrounding ejecta environment into a quasi-thermal emission.

To correctly interpret KN spectra, accurate models require not only hydrodynamical and nucleosynthesis simulations, but also a complex set of physical inputs, ranging from nucleosynthesis yields to opacity. In this context, atomic calculations of energy levels, line strengths, and transitions are essential ingredients to correctly estimate the opacity and link specific atomic species to observable

 doi:10.20944/preprints202604.1298.v1

features. These represent the main challenges to provide critical information not yet well understood concerning the physics of the merger, the nucleosynthetic pathways that occur, and the KN emission itself.

The majority of studies in the literature focused on modelling the KN in a late epoch (> 2 days), investigating the atomic properties and opacities of lanthanides and actinides [18–23]. However, works of the last decade [17,19,24–26] have highlighted that light r-process elements are very abundant in the early phases of a KN evolution and that during this phase they play a crucial role in spectral characterisation. Since much less literature has investigated this aspect, the goal of this work is to fill the gap in the available atomic data for lighter elements. These elements are generally more accessible and safer to handle in laboratory environments, making them particularly suitable for experimental studies. In this context, selenium and zirconium are among the primary candidates to be investigated in PANDORA (Plasma for Astrophysics Nuclear Decay Observation and Radiation for Archaeometry) [27], a magnetic trap facility currently under construction at the INFN - Laboratori Nazionali del Sud in Italy. A detailed study of atomic data, transition properties, and opacities has already been carried out for selenium [26]. Therefore, this work investigates zirconium (Zr) atomic calculations, as the availability of reliable atomic data is essential in view of future PANDORA measurements.

Following the established methodology adopted for selenium, this work focuses on atomic calculation of Zr I-IV in the framework of the early stage KN scenario (< 2 days). Beside experimental purposes, Zr is selected because it also represents one of the most abundant light r-process elements produced at early KN emission [28–30]. Zirconium atomic calculations are performed using the `GRASP2018` (general relativistic atomic structure package) code [31], whose computational procedure is discussed and reported in Section 2. `GRASP2018` is based on the fully relativistic (four-component) multi-configuration Dirac-Hartree-Fock (MCDHF) method [32,33]. It has become a widely-used code in atomic spectroscopy, with many applications in solar, stellar, and plasma physics. The code includes several additional routines such as relativistic configuration interaction (RCI), angular integrations with the second quantisation formalism [34,35], Breit interaction and also many-body quantum electrodynamics (QED) effects.

In atomic calculations, orbital correlations are essential to improve energy levels and transitions [36,37]. In view of this, the goal of this work is to estimate energy levels and transitions of Zr I-IV by including different types of orbital correlations in the electron configurations (ECs) forming the multi-reference (MR) sets. The calculations aim to get as close as possible to the `NIST ASD` (National Institute of Standards and Technology Atomic Spectra Database) [38], which serves as the main reference, and to evaluate how much these results deviate from those reported in the literature [39]. Moreover, the analysis assesses the intrinsic complexity of the Zr atomic calculations in `GRASP2018`. It is emphasised how sensitive the results are to the choice of both input parameters and computational procedure, together with the type of orbital correlations included. The entire analysis and results are presented in Sect. 3. Finally, these new Zr I-IV atomic data are now integrated and accessible on the `MARTINI` platform [26] to help the community shed light on the complex atomic calculations for KN modelling.

2. Materials and Methods

Zr is a light r-process element bound to the lanthanide-poor components of the post-mergers ejecta that dominate the early blue emission of a KN [28–30]. It is very abundant in the early phases ($\sim$ 10% of the total mass) [26,30] and, due to its moderate atomic structure complexity, it stands as one of the most interesting and feasible candidates among the light r-process element to be computationally studied. Moreover, in the KN early stage scenario (< 2 days), densities do not vary significantly [40], internal collisional processes dominate, and the environment is effectively thermalised, leading to high ionisation states of all elements of the ejecta. In this context, it is reasonable to assume local thermodynamic equilibrium and include higher ionisation states, in addition to neutral [19,39,41]. In view of this, beside Zr I, also Zr II, Zr III, and Zr IV were considered in the analysis.

 doi:10.20944/preprints202604.1298.v1

An important note is that GRASP2018 performs a single run per element per ionisation state. Therefore, every time an ionisation stage is calculated, a corresponding MR set of ECs must be defined. In this Zr study, two MR configurations were considered for each ionisation state. The two sets were constructed to investigate the impact that orbital correlations have on the atomic energy structure. For this reason, one set, labeled 'MR A', included all three types of orbital correlations (i.e. core-core (CC), core-valence (CV), and valence-valence (VV) correlations) for each ionisation stage (see Table A1). The other set, identified as 'MR B', only included VV correlations (see Table A2). All ECs of the MR sets are listed in Appendix A. A direct comparison between the two MR sets provides insight into how the inclusion or neglect of correlation influences the resulting energy levels. The two MR sets are also constructed by assuming a different fixed core in the ECs. As can be seen in Table A1, in MR A the Ar core is kept frozen (i.e. [Ar]). Moreover, the 3d and 4s shells are closed, while beyond 4p, all shells are treated as interactive for correlations and active for possible excitations. Instead, the fixed core for MR B is Kr (i.e. [Kr], see Table A2) with correlations and excitations allowed from the 4d shell. Once the MR sets are defined, angular integration and the radial wave function estimation were performed, followed by the MCDHF method to retrieve the numerical representation of the atomic state function.

The last part of the calculation was related to the RCI and Breit interaction, both implemented to optimise the precision of the results. In MR B, a single layer with virtual orbitals up to n-quantum number equal to seven was considered, while for MR A, a different approach was applied to the calculation. Specifically, in MR A, the RCI was implemented using a step-by-step procedure of optimisation through three different layers (i.e. L1, L2, and L3; see Table A3). Finally, energy levels and transitions were calculated considering single and double (SD) excitations.

3. Results and Discussion

The analysis is restricted only to the bound-state energy levels because bound-bound transitions dominate in KN [25,39,42,43]. Figure 1 shows the energy levels of Zr I-IV generated from MR A and MR B.

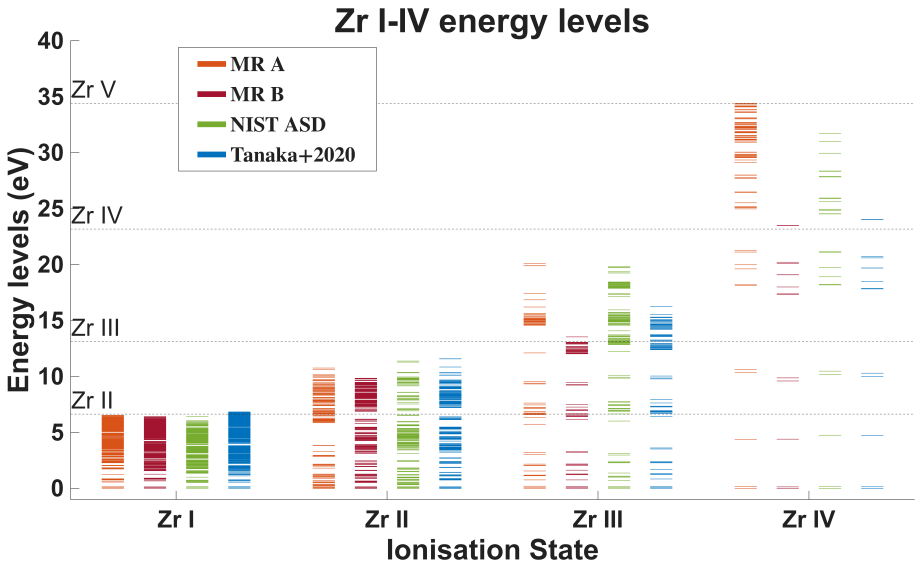

Figure 1. Zr I-IV energy levels of MR A and MR B compared with NIST ASD. The plot also includes a literature reference [39] for a consistent evaluation, and the dashed lines indicates the ionisation threshold for each Zr degree.

In the plot, NIST ASD and an example from the literature of Zr I-IV energy levels [39] are also shown. To validate the precision of the results, an uncertainty on the energy levels was calculated. The criterion consisted of computing the mean relative differences, $\Delta E_{\mathrm{rel}}(\%)$, between the predicted energy levels, E^{pred}, and those reported in the NIST ASD, E^{NIST}, to assess how much Zr I-IV calculations of MR A and MR B deviated from NIST ASD. This method was also applied to the literature data [39],

 doi:10.20944/preprints202604.1298.v1

as an example, to verify how much the Zr calculations presented in this work were consistent. The uncertainty was calculated with the following equation [37]:

$$\Delta E_{\rm rel}(\%) = \frac{|\overline{\Delta E}|}{E} \times 100 = \frac{\sum |\Delta E|/E}{N} \times 100 = \frac{\sum |E^{\rm NIST} - E^{\rm pred}|/E^{\rm NIST}}{N} \times 100, \quad (1)$$

where N represents the number of energy levels in common between the models. The energy levels discrepancies are reported in Table 1.

Table 1. Zr I-IV energy levels uncertainty of MR A, B and literature reference [39] compared to NIST ASD.

Zr	MR A	MR B	Tanaka+,2020	#levels
Degree	$\Delta E_{\rm rel}$ (%)	$\Delta E_{\rm rel}$ (%)	$\Delta E_{\rm rel}$ (%)	N
I	20.34	34.75	14.47	22
II	13.78	30.54	54.51	25
III	6.38	9.83	9.04	26
IV	1.67	5.72	2.42	12

Several insights emerge from Table 1. First of all, it shows that the energy levels obtained with MR A are more precise and closer to the NIST ASD than MR B. Specifically, Zr III and IV show an uncertainty below 7%, with results that are almost twice the times better than MR B. In the case of Zr I and II, the uncertainty is higher (> 12%), but it still proves to be twice or even three-times better than the one predicted by MR B. These results demonstrate that the only use of the VV correlation in MR is not enough to produce accurate estimates of energy levels. Instead, the inclusion of all three types of correlations (i.e. CC, CV, and VV) as in MR A (see Table A1) is necessary to achieve good precision. Table 1 further demonstrates that RCI calculations significantly affect the precision of the results. Specifically, Table A3 shows that the optimisation of the atomic structure of MR A was performed in three successive steps, preserving the symmetry between even and odd parity while increasing the principal quantum number by one at each iteration. In contrast, Table A4 indicates that the MR B optimisation was performed using only a single layer that does not preserve the orbital symmetry between even and odd configurations. This asymmetry in the calculations led to a less reliable procedure and, consequently, to less accurate estimates of the energy levels as confirmed by Table 1.

From the comparison with the literature example, Table 1 shows that MR A results of Zr II, III and IV are closer to the NIST ASD values, while Zr I deviates significantly. This indicates that the calculation strategy adopted for Zr I is still not enough to guaranty good precision on the energy levels. In view of this, future refinements on both MR set and computational strategy are required. From Table 1, it also emerges that with an increase in the ionisation degree, the precision of the energy levels improves. This behaviour is expected, as the reduction in the number of electrons leads to weaker electron correlation between shells that simplifies the calculations. Furthermore, Table 1 shows that the error evaluation for each ionisation stage is based on a different number of levels, N. The reason lies in several factors, including the difficulty in identifying the specific level and the limited availability of data. Specifically, GRASP2018 performs a conversion from jj-coupling to LS-coupling [44,45] to enable a direct comparison of level labels with NIST ASD (this LS-based identification is approved by the atomic theory community).

However, not all atomic codes have this transformation, with the consequence that labels for each level are often not explicitly reported. As a result, it becomes difficult to establish a consistent correspondence between all models calculations. Concerning the limited availability of data, this issue is clearly visible in Zr IV of Figure 1. In this case, a mismatch in the total number of energy levels predicted by MR A, NIST ASD, and the literature example is clearly visible, affecting the resulting precision and restricting the analysis to only a few energy levels in common.

 doi:10.20944/preprints202604.1298.v1

Concerning the Zr IV results, Figure 1 shows that the MR A calculations predict a larger number of bound-state energy levels than those reported in the NIST ASD. This indicates that the inclusion of $4p^5\{4d, 5s, 5p\}$ in ECs leads to additional energy levels, which may have a significant impact on the calculation of bound–bound transitions for KN. Therefore, MR A calculations for Zr I-IV provide a more complete energy level structure compared to the data currently available in both NIST ASD and literature.

The final part of the work concerned the evaluation of bound-bound transitions. Since the results of Table 1 proved that the energy level structure of MR A was more accurate and precise than MR B, bound-bound transitions were calculated only for MR A. The results are reported in Figure 2.

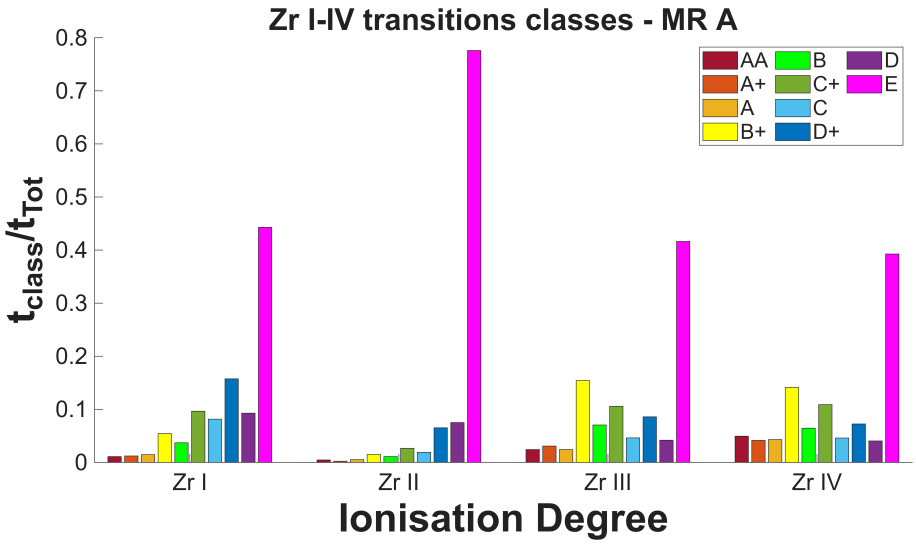

Figure 2. Zr I-IV bound-bound transitions of MR A. The coloured bars indicate an evaluation of the transitions, based on the wave function accuracy. Class AA indicates high wave function accuracy, while class E the lowest.

The bars in Figure 2 are derived from a quantitative and qualitative evaluation method [37] that consists of evaluating the accuracy of the wave function that generates the transition. In this classification, class AA corresponds to transitions with highly accurate wave function, whereas class E represents the lowest level of accuracy. Following the same methodology adopted in the previous study of selenium [26], Figure 2 provides an additional hint on the quality of the Zr I-IV calculations. The classification demonstrates that class E transitions are still dominant in all ionisation stages, despite the fact that present results show an overall improvement with respect to literature data and a better agreement with the NIST ASD. This indicates that the inclusion of core correlation alone is insufficient to accurately estimate bound–bound transitions. Moreover, except for Zr II, a clear decrease in the fraction of class E transitions is observed with increasing ionisation stage. This trend is in agreement with the precision of the energy levels reported in Table 1, confirming that a reduction in the total number of electrons simplifies the evaluation of the wave function and enhances its accuracy. Consistently with Table 1, a higher accuracy in the energy structure reflects into improved transition properties. This interpretation is further supported by the case of Zr II, where Figure 2 shows a significantly higher proportion of class E transitions compared to the other ionisation stages. In view of the energy level results, this behaviour is expected, as the energy structure of Zr II exhibits a gap in the 4–6 eV range (see Figure 1). Such a gap leads to an inaccurate representation of the energy level structure, which in turn affects the quality of the wave functions and results in unreliable transitions. In conclusion, these results suggest that the atomic calculations of Zr III and IV were performed correctly, while additional refinements are required in Zr I and Zr II.

4. Conclusions

This work presented preliminary results concerning the atomic calculations of Zr I-IV energy levels and transitions in the framework of the kilonova modelling. The calculations were performed

 doi:10.20944/preprints202604.1298.v1

using GRASP2018 atomic code, highlighting the sensitivity of the atomic structure calculations to the choice of electron configurations and the treatment of orbital correlations. In the analysis, two different multi-reference configurations, namely MR A and MR B, were considered per each ionisation stage. Multi-reference A included the core-core, the core-valence and the valence-valence correlations, while multi-reference B only assumed the valence-valence correlation. From a detailed comparison with NIST ASD, the results of MR A were more precise than those of MR B, in every ionisation stage, with an uncertainty in the energy levels of about 7% for Zr III and IV, and 14% and 20% for Zr II and Zr I, respectively. The energy levels comparison proved that the inclusion of core correlations, together with a good RCI strategy, are needed to increase the precision of the results. Moreover, Zr IV results showed that the inclusion of additional ECs predicts a more complete energy level structure than available references, which could affect KN modelling. However, orbital correlations are not sufficient to achieve accurate atomic calculations, as demonstrated by the transition results. Specifically, through a qualitative and evaluation method, all the ionisation stages exhibit a large number of transitions whose wave functions are not correctly estimated. Although an improvement in wave function accuracy is observed with increasing ionisation stage, additional refinements on the atomic calculation are needed to enhance the quality of the transitions. These newly Zr atomic data are now accessible from the open access MARTINI platform.

Data Availability Statement: The zirconium data presented in this work are now accessible on the open access astrophysical platform MARTINI at https://martini.oa-abruzzo.inaf.it/.

Conflicts of Interest: The author declares that there are no conflicts of interest.

Abbreviations

The following abbreviations are used in this manuscript:

BNS	Binary Neutron Star
KN	Kilonova
MR	Multi-Reference
EC	Electron Configuration
CC	Core-Core
CV	Core-Valence
VV	Valence-Valence
GRASP2018	General Relativistic Atomic Structure Package 2018
NIST ASD	National Institute of Standards and Technology Atomic Spectra Database

Appendix A

Table A1. List of MR A ECs*.

Zr I		Zr II		Zr III		Zr IV	
Even	Odd	Even	Odd	Even	Odd	Even	Odd
$4p^6\,4d^2\,5s^2$	$4p^6\,4d^2\,5s\,5p$	$4p^6\,4d^2\,5s$	$4p^6\,4d\,5s\,5p$	$4p^6\,4d^2$	$4p^6\,4d\,5p$	$4p^6\,4d$	$4p^6\,5p$
$4p^6\,4d^3\,5s$	$4p^6\,4d^3\,5p$	$4p^6\,4d^3$	$4p^6\,4d^2\,5p$	$4p^6\,4d\,5s$	$4p^6\,5s\,5p$	$4p^6\,5s$	$4p^6\,4f$
$4p^6\,4d^4$		$4p^6\,4d\,5s^2$		$4p^6\,5s^2$	$4p^6\,4d\,4f$	$4p^6\,5d$	$4p^5\,5p\,5d$
$4p^6\,4d^2\,5p^2$		$4p^6\,4d\,5p^2$		$4p^6\,5p^2$	$4p^6\,5s\,4f$	$4p^5\,4d\,5p$	$4p^5\,4d\,5s$
				$4p^6\,5p\,4f$		$4p^5\,4d\,4f$	
						$4p^5\,5s\,5p$	
						$4p^5\,5s\,4f$	

* All EC starts with [Ar] $3d^{10}\,4s^2$, where [Ar] is the argon fixed core, and $3d^{10}$ and $4s^2$ are the non-interactive closed shells. The $4p^6$ electrons interact with the valence electrons, forming the core-core and core-valence correlations.

 doi:10.20944/preprints202604.1298.v1

Table A2. List of MR B ECs*.

Zr I		Zr II		Zr III		Zr IV	
Even	Odd	Even	Odd	Even	Odd	Even	Odd
$4d^2\,5s^2$	$4d^2\,5s\,5p$	$4d^2\,5s$	$4d\,5s\,5p$	$4d^2$	$4d\,5p$	$4d$	$5p$
$4d^3\,5s$	$4d^3\,5p$	$4d^3$	$4d^2\,5p$	$4d\,5s$	$5s\,5p$	$5s$	$4f$
$4d^2\,5s\,6s$	$4d\,5s^2\,5p$	$4d^2\,5d$	$4d^2\,6p$	$5s^2$	$4d\,4f$	$6s$	
$4d^3\,6s$	$4d^2\,5s\,6p$	$4d\,5s^2$		$4d\,5d$	$4d\,6p$	$6d$	
$4d^2\,5p^2$		$4d^2\,6s$		$4d\,6s$			

* All ECs assume the Kr core (i.e. [Kr] = $3d^{10}\,4s^2\,4p^6$) as fixed, non-interactive (i.e. no core correlations).

Table A3. RCI layers of MR A*.

	Zr I		Zr II		Zr III		Zr IV	
Layer	Even	Odd	Even	Odd	Even	Odd	Even	Odd
L_1	{6s,6p,5d}		{6s, 6p, 5d}		{6s,6p,5d,5f}		{6s,6p,5d,5f}	
L_2	{7s,7p,6d}		{7s, 7p, 6d}		{7s,7p,6d,6f}		{7s,7p,6d,6f}	
L_3	{8s,8p,7d}		{8s, 8p, 7d}		{8s,8p,7d,7f}		{8s,8p,7d,7f}	

* Optimisation was achieved by incrementing the principal quantum number by one for each layer. All ionisation stages respected the same orbital symmetry between even and odd parity.

Table A4. RCI layers of MR B*.

	Zr I		Zr II		Zr III		Zr IV	
Layer	Even	Odd	Even	Odd	Even	Odd	Even	Odd
L_1	{7s,6p,5d}	{6s,7p,5d}	{7s,6d}	{6s,7p,5d}	{7s,6d}	{6s,7p,5d,4f}	{7s,7d}	{6p,5f}

* Only one single layer was considered to calculate RCI. All ionisation stages did not respect the orbital symmetry between even and odd parity.

References

1. Abbott, B.P.; et al. Gravitational Waves and Gamma-Rays from a Binary Neutron Star Merger: GW170817 and GRB 170817A. *ApJL* **2017**, *848*, L13.
2. Corsi, A.; et al. Multi-messenger astrophysics of black holes and neutron stars as probed by ground-based gravitational wave detectors: from present to future. *Front. Astron. Space Sci.* **2024**, *11*.
3. Lattimer, J.M.; Schramm, D.N. Black-hole-neutron-star collisions. *ApJ* **1974**, *192*, L145.
4. Cowan, J.J.; et al. Origin of the heaviest elements: The rapid neutron-capture process. *Rev. Mod. Phys.* **2021**, *93*, 015002.
5. Abbott, B.P.; et al. Multi-messenger Observations of a Binary Neutron Star Merger*. *ApJL* **2017**, *848*, L12.
6. He, X.B.; et al. GRB 170817A: a short GRB seen off-axis. *Res. Astron. Astrophys.* **2018**, *18*, 043.
7. Lyman, J.D.; et al. The optical afterglow of the short gamma-ray burst associated with GW170817. *Nat. Astron.* **2018**, *2*, 751–754.
8. Evans, P.A.; et al. SwiftandNuSTARobservations of GW170817: Detection of a blue kilonova. *Science* **2017**, *358*, 1565–1570.
9. Kasliwal, M.M.; et al. Illuminating gravitational waves: A concordant picture of photons from a neutron star merger. *Science* **2017**, *358*, 1559–1565.
10. McCully, C.; et al. The Rapid Reddening and Featureless Optical Spectra of the Optical Counterpart of GW170817, AT 2017gfo, during the First Four Days. *ApJL* **2017**, *848*, L32.
11. Pian, E.; et al. Spectroscopic identification of r-process nucleosynthesis in a double neutron-star merger. *Nature* **2017**, *551*, 67–70.
12. Smartt, S.J.; et al. A kilonova as the electromagnetic counterpart to a gravitational-wave source. *Nature* **2017**, *551*, 75–79.
13. Soares-Santos, M.; et al. The Electromagnetic Counterpart of the Binary Neutron Star Merger LIGO/Virgo GW170817. I. Discovery of the Optical Counterpart Using the Dark Energy Camera. *ApJL* **2017**, *848*, L16.

 doi:10.20944/preprints202604.1298.v1

14. Utsumi, Y.; et al. J-GEM observations of an electromagnetic counterpart to the neutron star merger GW170817. *PASJ* **2017**, *69*.
15. Radice, D.; et al. The Dynamics of Binary Neutron Star Mergers and GW170817. *Annu. Rev. Nucl. Part. Sci.* **2020**, *70*, 95–119.
16. Kasen, D.; et al. Origin of the heavy elements in binary neutron-star mergers from a gravitational-wave event. *Nature* **2017**, *551*, 80–84.
17. Metzger, B.D. Kilonovae. *Living Rev. Relativ.* **2019**, *23*.
18. Gillanders, J.H.; et al. Constraints on the presence of platinum and gold in the spectra of the kilonova AT2017gfo. *MNRAS* **2021**, *506*, 3560–3577.
19. Banerjee, S.; et al. Diversity of Early Kilonova with the Realistic Opacities of Highly Ionized Heavy Elements. *ApJ* **2024**, *968*, 64.
20. Fontes, C.J.; et al. Actinide opacities for modelling the spectra and light curves of kilonovae. *MNRAS* **2023**, *519*, 2862–2878.
21. Flörs, A.; et al. Opacities of singly and doubly ionized neodymium and uranium for kilonova emission modeling. *MNRAS* **2023**, *524*, 3083–3101.
22. Carvajal Gallego, H.; et al. Overview of the contributions from all lanthanide elements to kilonova opacity in the temperature range from 25 000 to 40 000 K. *A&A* **2024**, *685*, A91.
23. Kato, D.; et al. Systematic opacity calculations for kilonovae – II. Improved atomic data for singly ionized lanthanides. *MNRAS* **2024**, *535*, 2670–2686.
24. Villar, V.A.; et al. The Combined Ultraviolet, Optical, and Near-infrared Light Curves of the Kilonova Associated with the Binary Neutron Star Merger GW170817: Unified Data Set, Analytic Models, and Physical Implications. *ApJL* **2017**, *851*, L21.
25. Banerjee, S.; et al. Simulations of Early Kilonova Emission from Neutron Star Mergers. *ApJ* **2020**, *901*, 29.
26. Bezmalinovich, M.; et al. The MARTINI platform. I: Se I-X atomic calculation and expansion opacity for early stage kilonova spectral analysis. *A&A* **2026**, *in press*.
27. Mascali, D.; et al. A Novel Approach to β-Decay: PANDORA, a New Experimental Setup for Future In-Plasma Measurements. *Universe* **2022**, *8*, 80.
28. Nedora, V.; et al. Spiral-wave Wind for the Blue Kilonova. *ApJL* **2019**, *886*, L30.
29. Perego, A.; et al. Production of Very Light Elements and Strontium in the Early Ejecta of Neutron Star Mergers. *ApJ* **2022**, *925*, 22.
30. Vescovi, D.; et al. Neutron-capture measurement candidates for the r-process in neutron star mergers. *Front. Astron. Space Sci.* **2022**, *9*.
31. Froese Fischer, C.; et al. GRASP2018—A Fortran 95 version of the General Relativistic Atomic Structure Package. *Comput. Phys. Commun.* **2019**, *237*, 184–187.
32. Grant, I.P. *Relativistic Quantum Theory of Atoms and Molecules*; Springer New York, 2007.
33. Fischer, C.F.; et al. Advanced multiconfiguration methods for complex atoms: I. Energies and wave functions. *J. Phys. B* **2016**, *49*, 182004.
34. Gaigalas, G.; et al. Program to calculate pure angular momentum coefficients in -coupling. *Comput. Phys. Commun.* **2001**, *139*, 263–278.
35. Gaigalas, G.; et al. JJ2LSJ Transformation and Unique Labeling for Energy Levels. *Atoms* **2017**, *5*, 6.
36. Radžiūtė, L.; Gaigalas, G. Energy levels and transition properties for As-like ions Se II, Br III, Kr IV, Rb V, and Sr VI. *At. Data Nucl. Data Tables* **2022**, *147*, 101515.
37. Kitovienė, L.; et al. Theoretical Investigation of the Ge Isoelectronic Sequence. *J. Phys. Chem. Ref. Data* **2024**, *53*.
38. Kramida, A.; Ralchenko, Y. NIST Atomic Spectra Database, NIST Standard Reference Database 78, 1999.
39. Tanaka, M.; et al. Systematic opacity calculations for kilonovae. *MNRAS* **2020**, *496*, 1369–1392.
40. Pognan, Q.; et al. NLTE effects on kilonova expansion opacities. *MNRAS* **2022**, *513*, 5174–5197.
41. Banerjee, S.; et al. Opacity of the Highly Ionized Lanthanides and the Effect on the Early Kilonova. *ApJ* **2022**, *934*, 117.
42. Kasen, D.; et al. Opacities and spectra of the r-process ejecta from neutron star nergers. *ApJ* **2013**, *774*, 25.
43. Tanaka, M.; Hotokezaka, K. Radiative transfer simulations of neutron star merger ejecta. *ApJ* **2013**, *775*, 113.

 doi:10.20944/preprints202604.1298.v1

44. Gaigalas, G.; et al. Analytical expressions for special cases of LS-jj transformation matrices for a shell of equivalent electrons. *Lith. J. Phys.* **2001**, *41*, 226–231.
45. Gaigalas, G.; et al. LS–jj transformation matrices for a shell of equivalent electrons. *At. Data Nucl. Data Tables* **2003**, *84*, 99–190.